RSC Advances

ROYAL SOCIETY OF CHEMISTRY

www.rsc.org/advances

Journal Name

ARTICLE

A Novel $Li_2Mn_{2.9}Ni_{0.9}Co_{0.2}O_8$ Spinel Composite Interweaved with Carbon Nanotube Architecture as Lithium Battery Cathode

Received 00th January 20xx,
Accepted 00th January 20xx

DOI: 10.1039/x0xx00000x

www.rsc.org/

Remith Pongilat [a] and Kalaiselvi Nallathamby *[a]

$Li_2Mn_{2.9}Ni_{0.9}Co_{0.2}O_8$ spinel nanoflakes, synthesized for the first time using a template assisted co-precipitation method form interconnected composite with MWCNT and demonstrate excellent lithium intercalation/de-intercalation performance upon cycling. As cathode, $Li_2Mn_{2.9}Ni_{0.9}Co_{0.2}O_8$/MWCNT composite exhibits exceptionally interesting properties such as high specific capacity, acceptable rate performance upto 5C rate condition, appreciable coulombic efficiency and better cycling stability compared with that of the pristine $Li_2Mn_{2.9}Ni_{0.9}Co_{0.2}O_8$, especially due the effect of interweaved MWCNT. A steady state discharge capacity of ~210 mAh g^{-1} at a current density of 0.1C has been achieved with $Li_2Mn_{2.9}Ni_{0.9}Co_{0.2}O_8$/MWCNT composite cathode against an inferior capacity of 135 mAh g^{-1} exhibited by pristine $Li_2Mn_{2.9}Ni_{0.9}Co_{0.2}O_8$ cathode. Even at a discharge rate of 1C, the title cathode, belonging to the category of spinel oxides delivers a high capacity of 100 mAh g^{-1} after 100 cycles, which is noteworthy. The encouraging electrochemical properties result from the synergistic effect of enhanced high lithium-ion diffusion kinetics of nanosized flakes of $Li_2Mn_{2.9}Ni_{0.9}Co_{0.2}O_8$ and the high electronic conductivity of multiwalled carbon nanotube network. The current findings leave ample scope to tailor make and exploit wide variety of solid solutions based on $Li_2MMn_3O_8$ (M-Transition metal) family spinel cathodes, possibly for high capacity and high rate lithium battery applications, especially when deployed in the form of a composite with MWCNT.

Introduction

In the modern green energy revolution context, rechargeable lithium batteries are the choicest and globally accepted energy storage media for application in emission free vehicles and portable electronic devices [1-5]. Even though these lithium batteries are capable of exhibiting better electrochemical performance than other battery systems, their safety, lifetime, energy density and high voltage characteristics are required to be improved to meet with the energy needs of consumer market based applications. The commercialized $LiCoO_2$ suffers from a lower potential value of 3.7 V and its questionable safety, especially above 4.2 V has triggered an ever pressing need to explore few other novel, safe and economically viable cathode materials [6-9]. Particularly, demand for lithium-ion batteries with alternative cathode materials is augmented, thus provoking the identification and development of cathode material, bestowed with high electronic and ionic conductivity, high working voltage, appreciable stability and cycleability as the need of the hour.

After the successful exploration of lithium rich layered oxide materials, *viz.* $xLi_2MnO_3 \cdot (1-x)LiMO_2$ (M= Mn, Ni, Co) as high capacity cathode materials, researchers, including our group are extensively trying to develop newer cathode materials, capable of exhibiting capacity as high as 200 mAh g^{-1} [10-13]. However, these Li_2MnO_3 stabilized cathode materials suffer from large irreversible capacity loss behaviour in the first formation cycle that prevents their commercial exploitation. On the other hand, spinel type transition metal oxides of the general formula AB_2O_4 form a large class of materials, wherein the inherent and diverse properties ensure their wide application in areas such as lithium-ion batteries, catalysis and supercapacitors [14-18]. Depending upon the structure and composition, spinel oxides exhibit high electronic and ionic conductivity and demonstrate themselves as potential cathode materials. Among them, $LiMn_2O_4$ and nickel doped $LiMn_2O_4$ are widely studied spinel materials, which are capable of delivering even second level charge capability in aqueous electrolytes [19-23]. Herein, facile lithium ion diffusion through the three dimensional ion channels and the high electrochemical potential of these spinel type cathodes make them more suitable for practical applications.

Towards this direction, quite different from the conventional and popularly known AB_2O_4 type of 4V spinel cathodes, yet another class of spinel compounds with a general formula of $Li_2MMn_3O_8$ (M= Cu, Co, Ni and Fe) are capable of performing as lithium battery cathode over 4.5 V region, depending upon the transition metal and thus gain importance as high voltage cathode materials [24-30]. These

a. *Electrochemical Power Sources Division*
CSIR- Central Electrochemical Research Institute
Karaikudi- 630 006, India
E-mail: kalaiselvicecri@gmail.com

† Electronic Supplementary Information (ESI) available: Additional information includes FTIR spectra of pristine and composite material, first cycle charge/discharge voltage profile of composite and room temperature conductivity curves. See DOI: 10.1039/x0xx00000x

spinels, although identical to $LiMn_2O_4$ spinel are bestowed with an entirely different cation ordering in the octahedral sites, *i.e.*, 1:3 instead of 1:1 ordering (found with AB_2O_4 type) and hence could not be considered as simple binary spinels [24]. H. Kawai *et.al.*, reported for the first time that $Li_2CoMn_3O_8$ cathode exhibits a very high working voltage, c.a. 5 V with an excellent cycling stability [25]. Subsequently, the same authors reported on the application of $Li_2FeMn_3O_8$ cathode with a voltage plateau at 4.9 V [26]. Even though few other reports are available on the high voltage characteristics of $Li_2MMn_3O_8$ class of compounds, the long term cycleability and their suitability for high rate applications are yet to be explored. In general, electrolyte decomposition, structural distortion and cation ordering based issues upon extended and high rate cycling are certain hampering parameters, due to which the intriguing behavior of such 5 V spinels poses innumerable challenges. Towards this direction, synthesis-structure-property relationship pertinent to customised $Li_2CoMn_3O_8$ based spinel cathode formulations needs to be investigated in detail, as it remains as the less studied area of research.

Of late, reports on spinel composite cathodes provide a tangible platform and enormous scope to fine tune the properties of native spinel cathodes to best suit with the requirements of high capacity cathode for rechargeable lithium batteries. Similarly, provision of shorter lithium diffusion pathways by reducing the particle size to nanoscale along with the conductive surface modification has been reported to address the rate performance related issues associated with spinel cathodes. Recently, H. K. Noh et.al., proposed a simple strategy to harvest a capacity of 220 mAh g^{-1} from lithium manganese oxide at a cut off voltage of 2.5 V from the composite consisting of flexible skinny graphitic layer [31]. Similarly, S. Lee et.al., demonstrated the high energy and high power capability of single crystal $LiMn_2O_4$ clusters by surface modification with carbon coating [32]. From these reports, it is clear that surface modification with a suitable carbon might provide a facile electron transporter and a stable spinel structure at the 3 V region. However, no report on the possibility of qualifying a $Li_2MMn_3O_8$ spinel, otherwise known as 5 V cathode for high capacity and/or high rate lithium battery applications is available. In this regard, the current piece of work assumes significant importance, as it demonstrates for the first time the suitability of $Li_2MMn_3O_8$ type of high voltage cathodes for high capacity and rated capacity applications, especially with the carefully chosen and tailor-made formulation of solid solution.

Herein, we report a simple solution based synthesis of interconnected $Li_2Mn_{2.9}Ni_{0.9}Co_{0.2}O_8$/MWCNT composite material by interweaving the spinel $Li_2Mn_{2.9}Ni_{0.9}Co_{0.2}O_8$ compound within the multiwalled carbon nanotubes matrix. This newly designed heterostructured material offers significantly high discharge capacity and better rate performance, facilitated mainly by the interconnecting and the conductive MWCNT network. In other words, MWCNT provides the desirable carbon wiring and improves the conductivity, thereby increasing the capacity and rate capability. Herein, pristine $Li_2Mn_{2.9}Ni_{0.9}Co_{0.2}O_8$ has been prepared by a template assisted co-precipitation method (see the Experimental Section for details). Without requiring any complex synthesis procedure or experimental conditions, the as-prepared $Li_2Mn_{2.9}Ni_{0.9}Co_{0.2}O_8$, especially when deployed in the form of $Li_2Mn_{2.9}Ni_{0.9}Co_{0.2}O_8$/MWCNT composite cathode demonstrates excellent electrochemical properties, such as a high specific capacity of 210 mAh g^{-1} at 0.1C current rate and an appreciable capacity of 100 mAh g^{-1} at the end of the 100th cycle at 1C current rate have been observed, which is the highlight of the study.

2. Experimental Section

2.1. Synthesis of $Li_2Mn_{2.9}Ni_{0.9}Co_{0.2}O_8$/MWCNT composite

All the reagents used were of analytical grade (Sigma-Aldrich and Alfa-Aesar) and were used without further purification. In a typical synthesis, polyethyleneimine (M_W=1300) (4 mL) was added to deionised water (50 mL) and stoichiometric ratio of Mn, Co and Ni precursors was mixed with magnetic stirring. After the mixture became transparent, 2M KOH was added drop wise until the solution became chocolate brown colour. The solution was left with overnight stirring and the obtained brown colour precipitate was centrifuged, washed three times with deionised water and absolute alcohol (to completely remove uncomplexed polyethyleneimine) and dried in a hot air oven at 120 °C for 12 h. The dried powder was subsequently mixed with LiOH and ethanol with the help of a mortar and pestle and further calcined at 450 °C for 6 h. To the obtained powder, MWCNTs (5 wt. %) were added and dispersed by ultrasonication in ethanol for 2 h. The mixture was dried at 80 °C for 10 h to get the final $Li_2Mn_{2.9}Ni_{0.9}Co_{0.2}O_8$ /MWCNT composite.

2.2. Material Characterization

Phase purity, crystallinity and structural stability of $Li_2Mn_{2.9}Ni_{0.9}Co_{0.2}O_8$/MWCNT compound were examined using Bruker D8 advance powder X-ray diffractometer. Unitcell lattice constants were calculated from the XRD data using "unitcell" software. Field emission scanning electron microscopy (Zeiss Field Emission Scanning Electron Microscope) was used to investigate the morphology of the sample and high resolution transmission electron microscopy (JEOL JEM 2100 Transmission Electron Microscope) was used to determine the particle size and further for the recording of SAED pattern. The Raman spectrum was recorded on Renishaw InVia Raman spectrometer with an argon ion laser and charge coupled device detector. FTIR spectra were recorded on Bruker Tensor 27 FT-IR Spectrometer in the range of 400-4000 cm^{-1} in the transmittance mode. The conductivity measurements were made using Wayne Kerr 6500 P high-frequency LCR meter. Powder samples were made into pellets of 2 mm thickness and 10 mm diameter. Conductive silver paste was applied on both sides of the pellets and sandwiched between stainless steel blocking electrodes to measure the conductivity.

2.3. Electrochemical Studies

CR 2032 coin type cells (Hohsen) were used for evaluating the electrochemical performance of $Li_2Mn_{2.9}Ni_{0.9}Co_{0.2}O_8$/MWCNT

composite cathode. Coin cells were assembled in a glovebox (Mbraun) under argon atmosphere. The working electrode was fabricated by mixing the active material, acetylene black and polyvinylidene fluoride binder in the weight ratio of 80:10:10. Lithium ribbon was used as both counter and reference electrode and Celgard membrane was used as the separator. 1M solution of $LiPF_6$ in 1:1 (v/v) mixture of ethylene carbonate and diethyl carbonate was used as the electrolyte. The charge-discharge studies were performed on an Arbin battery tester in the voltage range of 2.0- 4.9 V at room temperature. Electrochemical impedance spectroscopy (EIS) measurements were carried out on a Biologic VMP3 electrochemical work station in the frequency ranging from 0.25 MHz to 10 mHz with an amplitude voltage of 10 mV at room temperature.

3. Results and Discussion

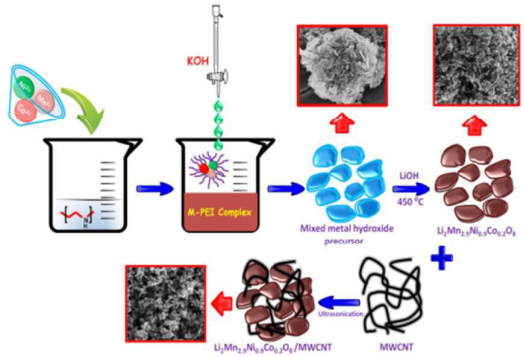

Scheme 1. Synthesis of $Li_2Mn_{2.9}Ni_{0.9}Co_{0.2}O_8$/MWCNT heterostructures by co-precipitation method.

Scheme 1 illustrates the synthesis approach of $Li_2Mn_{2.9}Ni_{0.9}Co_{0.2}O_8$ by a simple template assisted co-precipitation method. Polyethyleneimine (PEI) has been used as the template in this synthesis. It is well known that polyethyleneimine has the ability to form complexes with wide variety of metal ions [33-35]. The metal ions initially react with PEI molecules during stirring and form metal- PEI complexes. On adding potassium hydroxide, these metal ions are precipitated as mixed metal hydroxide. The separated metal hydroxide precursor has a flaky morphology, as evidenced by Figure 1a and b. The homogenous distribution of metal hydroxide nanoflakes is believed to result from the attachment of the polyelectrolyte (PEI) on the surface of the metal, which in turn reduces the size of the particles by preventing the coalescence of particles due to the repulsive interaction between same charges on the polyethyleneimine. Calcination of this precursor after mixing with LiOH leads to the formation of $Li_2Mn_{2.9}Ni_{0.9}Co_{0.2}O_8$ nanoflakes as the final product (Figure 1c and d). The flaky morphology of the precursor has been preserved even after calcination at 450 °C. The flakes are uniformly distributed in size, possessing a width of 200 nm and an average thickness of 15-20 nm. The multiwalled carbon nanotube interweaved heterostructure has been prepared by dispersing $Li_2Mn_{2.9}Ni_{0.9}Co_{0.2}O_8$ nanoflakes and MWCNT in ethanol with the help of a simple sonication process. Solvent evaporation from this mixture upon drying forms the spinel $Li_2Mn_{2.9}Ni_{0.9}Co_{0.2}O_8$/MWCNT composite material. The morphology of the spinel $Li_2Mn_{2.9}Ni_{0.9}Co_{0.2}O_8$/MWCNT composite material is displayed in Figure 1 e-f, which evidences the presence of heterostructured material, consisting of spinel nanoparticles interconnected with each other through MWCNT network. The conductive carbon wiring offered by MWCNTs enhances the electronic conductivity of pristine $Li_2Mn_{2.9}Ni_{0.9}Co_{0.2}O_8$ material and thereby improving the electrochemical performance of $Li_2Mn_{2.9}Ni_{0.9}Co_{0.2}O_8$/MWCNT composite cathode ultimately.

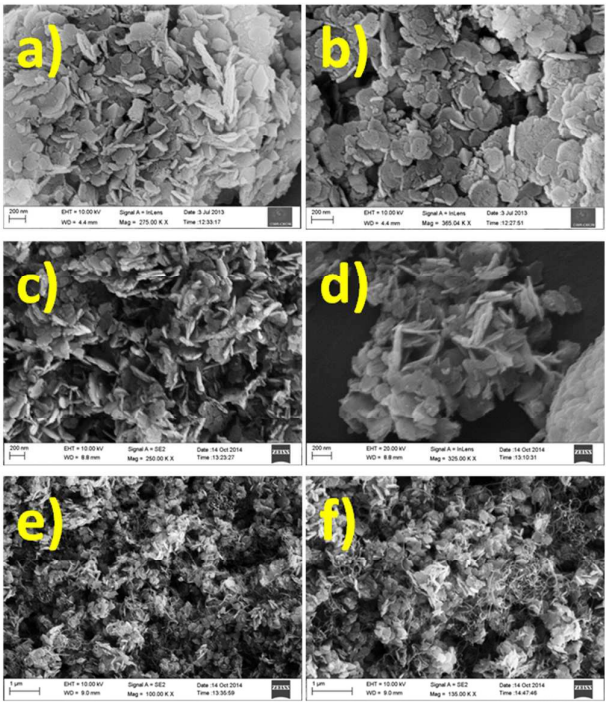

Figure. 1. FESEM images of (a and b) mixed metal hydroxide precursor, (c and d) pristine $Li_2Mn_{2.9}Ni_{0.9}Co_{0.2}O_8$ synthesized at 450 °C and (e and f) $Li_2Mn_{2.9}Ni_{0.9}Co_{0.2}O_8$/MWCNT composite at different magnifications, showing the presence of uniform network, formed out of multiwalled carbon nanotubes.

The morphology and particle size of the pristine and $Li_2Mn_{2.9}Ni_{0.9}Co_{0.2}O_8$/MWCNT composite are evident from the recorded HRTEM images. Figure 2 (a and b) evidences the presence of flakes possessing a thickness of 15- 20 nm and the diameter is 150-200 nm. High resolution image shows the presence of lattice fringes (Figure 2c and Figure S1), pertinent to the spinel $Li_2Mn_{2.9}Ni_{0.9}Co_{0.2}O_8$ framework and the SAED pattern confirms the polycrystalline nature of the spinel $Li_2Mn_{2.9}Ni_{0.9}Co_{0.2}O_8$ nanoflakes (Figure 2d). This observation has been corroborated by the recorded XRD pattern and Raman spectra (displayed in Figures 3 and Figures 4 respectively), which are the characteristics of spinel materials. Additionally, Figure 2 (c and d) confirms the crystalline nature of low temperature synthesized spinel nanoflakes, which is

quite interesting. The representative HRTEM images of $Li_2Mn_{2.9}Ni_{0.9}Co_{0.2}O_8$/MWCNT composite are displayed in Figure 2 (e and f), which is an indication that the multiwalled carbon nanotube networks interconnect the spinel nanoflakes, leading to possibly improved electronic conductivity and electrochemical properties.

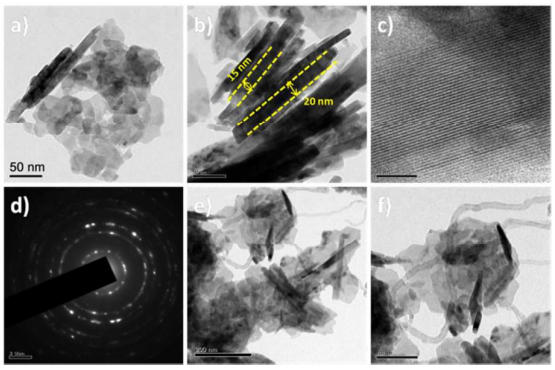

Figure. 2 (a and b) Low resolution HRTEM images of $Li_2Mn_{2.9}Ni_{0.9}Co_{0.2}O_8$ showing flaky morphology, (c) high resolution image showing the lattice fringes of spinel $Li_2Mn_{2.9}Ni_{0.9}Co_{0.2}O_8$, (d) SAED pattern showing the polycrystalline nature of $Li_2Mn_{2.9}Ni_{0.9}Co_{0.2}O_8$ compound and (e and f) carbon wiring found in $Li_2Mn_{2.9}Ni_{0.9}Co_{0.2}O_8$ with MWCNT

Figure 3 shows the powder XRD pattern of pristine $Li_2Mn_{2.9}Ni_{0.9}Co_{0.2}O_8$ compound prepared at 450 °C and the corresponding $Li_2Mn_{2.9}Ni_{0.9}Co_{0.2}O_8$/MWCNT composite. The XRD patterns match well with the *Fd3m* space group of the spinel compound, as per standard JCPDS card number: 802162 [36-38]. Intriguingly, no impurity peaks are found in the diffractogram and the lattice parameter value '*a*' has been calculated as 8.1869, which shows striking similarity with the reported results. Hence, it is understood that the reaction of LiOH with the metal hydroxide precursor at 450 °C produces phase pure $Li_2Mn_{2.9}Ni_{0.9}Co_{0.2}O_8$, wherein polyethyleneimine template has been removed completely during calcination and the metal hydroxide precursor has been ultimately transformed into the desired final product.

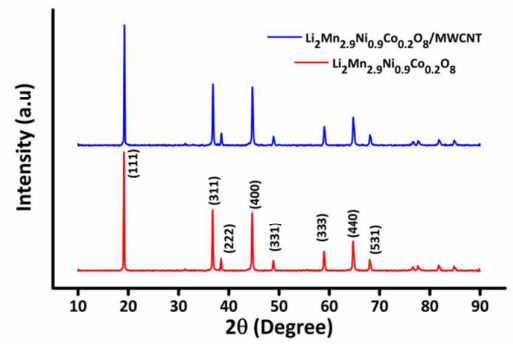

Figure. 3. XRD pattern of a) $Li_2Mn_{2.9}Ni_{0.9}Co_{0.2}O_8$ and b) $Li_2Mn_{2.9}Ni_{0.9}Co_{0.2}O_8$/MWCNT composite

It is well known that spinel compounds may possess two different types of arrangement of atoms with respect to the space groups, *viz., Fd3m* and $P4_332$. Discrimination of such crystallographic arrangement of space groups could be done by the careful analysis of local cation environment. It is in this context, a thorough analysis of the FTIR spectra and the complimentary Raman spectra assumes paramount importance, especially when the key information on the local cation environment and crystallographic arrangement of space group of spinel compounds is required. FTIR spectra of pristine $Li_2Mn_{2.9}Ni_{0.9}Co_{0.2}O_8$ and the corresponding composite (Supporting Information (SI), Figure S2**)** contain typical peaks

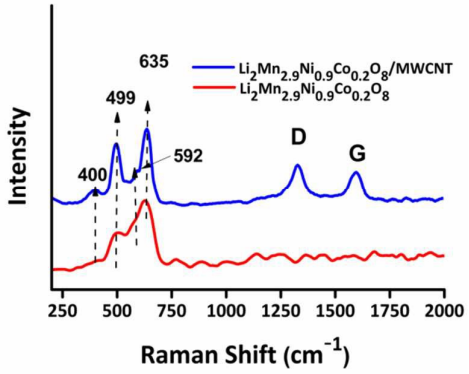

Figure. 4. Raman spectra of pristine $Li_2Mn_{2.9}Ni_{0.9}Co_{0.2}O_8$ and $Li_2Mn_{2.9}Ni_{0.9}Co_{0.2}O_8$/MWCNT composite (D and G bands of multiwalled carbon nanotubes are also indicated)

corresponding to those of Mn-O (626 cm^{-1}) and Ni-O (500 and 577 cm^{-1}) stretching vibrations [39]. Bands due to multiwalled carbon nanotubes are clearly visible around 1668 (C=O), 2925 (CH_3), 1582 (C-C), 1018 (C-O) and 3293 cm^{-1} (O-H). At this juncture, it is very difficult to differentiate the crystallographic arrangement of the spinel structure with two different space groups using FTIR spectra, whereas, Raman spectroscopy could be used to distinguish such space groups, apart from gaining information on the cation ordering in spinel compounds. Evidently, no splitting of signal has been found in the 550-600 cm^{-1} region in the Raman spectrum of bare and composite $Li_2Mn_{2.9}Ni_{0.9}Co_{0.2}O_8$/MWCNT material, which in turn confirms the presence of *Fd3m* space group, as inferred from the XRD pattern. The band at 635 cm^{-1} is due to the Mn-O stretching vibration (*A1g*) (oxidation state) and Ni-O stretching vibration is visible at 592 ($F2g^{(1)}$), 499 ($F2g^{(2)}$) and 400 cm^{-1} (*Eg*) [39]. Furthermore, Raman spectrum of the $Li_2Mn_{2.9}Ni_{0.9}Co_{0.2}O_8$/MWCNT composite (Figure 4) clearly shows the presence of characteristic D and G bands of multiwalled carbon nanotubes.

The electrochemical performance of $Li_2Mn_{2.9}Ni_{0.9}Co_{0.2}O_8$/MWCNT cathode has been evaluated by fabricating coin-type half cells with lithium metal as the counter and reference electrode. Figure 5a shows the cyclic voltammogram of $Li_2Mn_{2.9}Ni_{0.9}Co_{0.2}O_8$/MWCNT cathode, recorded at a scan rate of 0.1 mV s^{-1}. Generally, for nickel doped spinels, presence of Mn^{3+} related oxidation peak at 3.9-4.2 is barely detected [40,41]. By contrast, a broad peak due to

Mn^{3+}/Mn^{4+} couple is observed around 4.0 V (Figure 5a), indicating the presence of Mn^{3+}ions in the spinel framework. The peak above 4.6 V is due to the oxidation of nickel ions, as in the case of similar type of nickel doped spinel oxide, *viz.* $LiNi_{0.5}Mn_{1.5}O_4$. In other words, the oxidation peak at 4.7 V could be corroborated with the presence of $Ni^{2+/4+}$ redox couple. Basically, the presence of broad and unresolved peak shows the presence of less crystalline framework of nickel doped spinels. But in the case of $Li_2Mn_{2.9}Ni_{0.9}Co_{0.2}O_8$, prepared from the low temperature synthesis protocol, clear splitting of CV peak is observed, which is an indication of crystallinity of

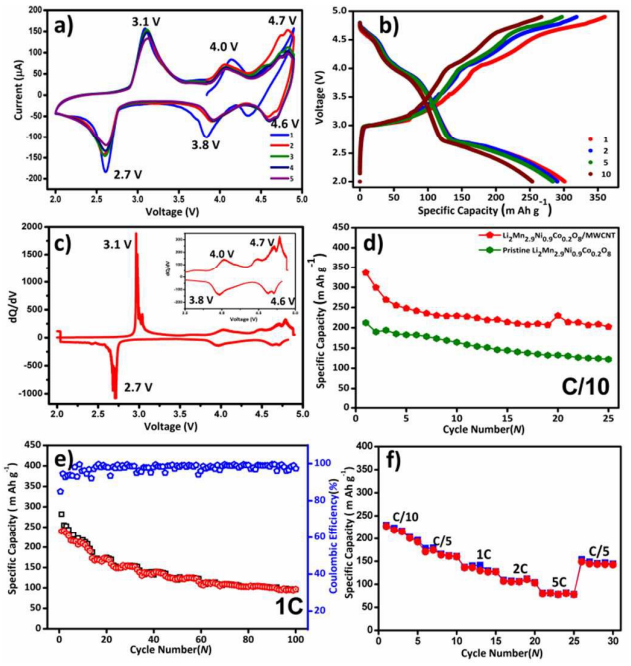

Figure. 5. (a) Cyclic voltammogram of $Li_2Mn_{2.9}Ni_{0.9}Co_{0.2}O_8$/MWCNT cathode recorded at a scan rate of 0.1 mV s^{-1} (b) galvanostatic charge/discharge curves recorded at 0.1C rate for the first ten cycles (c) dQ/dV profile of the second cycle (d) comparison of discharge capacity of $Li_2Mn_{2.9}Ni_{0.9}Co_{0.2}O_8$/MWCNT and pristine $Li_2Mn_{2.9}Ni_{0.9}Co_{0.2}O_8$ cathode (e) specific capacity and coulombic efficiency of $Li_2Mn_{2.9}Ni_{0.9}Co_{0.2}O_8$/MWCNT cathode upon progressive cycling at 1C rate and (f) rate capability behavior of $Li_2Mn_{2.9}Ni_{0.9}Co_{0.2}O_8$/MWCNT cathode

the title cathode [42]. Similarly, upon discharge, peaks corresponding to the reduction of Ni^{4+} and Mn^{4+} are visible at 4.6 and 3.8 V respectively. The transition from cubic to tetragonal phase occurs at a potential below 3.0 V during reduction that corresponds to the peak observed at 2.7 V. Subsequently, the cubic phase is found to get resumed during oxidation that takes place around 3.1 V (Figure 5a). Galvanostatic charge/discharge behavior of $Li_2Mn_{2.9}Ni_{0.9}Co_{0.2}O_8$/MWCNT cathode, recorded at a constant rate of 0.1C in the voltage range of 2.0 to 4.9 V is depicted in Figure 5b. The initial formation cycle of the $Li_2Mn_{2.9}Ni_{0.9}Co_{0.2}O_8$/MWCNT cathode is depicted in the supporting information Figure S3. The larger capacity values of the title cathode in the first few cycles are believed to be due to the occurrence of electrolyte oxidation at high voltage and structural re-organisation of the spinel framework above 4.5 V [43]. Further, the charge discharge capacity is found to get stabilised after ten cycles and a steady state reversible capacity of ~210 mAh g^{-1} has been exhibited by $Li_2Mn_{2.9}Ni_{0.9}Co_{0.2}O_8$/MWCNT cathode, which is noteworthy. However, the origin of the observed capacity obtained from a combination of intercalation/de-intercalation of lithium ions and the corresponding redox couples related to the presence of manganese and nickel ions could be better understood from the dQ/dV behavior of the title cathode. Figure 5c depicts the dQ/dV versus voltage curve of $Li_2Mn_{2.9}Ni_{0.9}Co_{0.2}O_8$/MWCNT cathode, obtained after the formation cycle. The dQ/dV behavior clearly demonstrates the involvement of series of electrochemical processes occurring at different voltages. There are three peaks observed at 3.1, 4.0 and 4.7 V, which are ascribed to the de-intercalation of lithium ions from cubic spinel structure. The peak at 4.0 V corresponds to the oxidation of Mn^{3+} ions and the strong redox peak located at 4.7 V is caused by the oxidation of Ni^{2+} to Ni^{4+}. In the reversible cycling process, peaks at 4.6 and 3.8 V, which are associated with the discharge process correspond to the reduction of respective redox couples aided by the reversible insertion of extracted lithium ions, which is consistent with the cyclic voltammetry results. Here again, presence of peak at 3.1 V upon oxidation and the one at 2.7 V during reduction substantiates the cubic-tetragonal conversion of $Li_2Mn_{2.9}Ni_{0.9}Co_{0.2}O_8$ spinel cathode.

The specific discharge capacity of $Li_2Mn_{2.9}Ni_{0.9}Co_{0.2}O_8$/MWCNT cathode as a function of cycle number has been compared with that of pristine $Li_2Mn_{2.9}Ni_{0.9}Co_{0.2}O_8$ (Figure 5d). We have observed that the $Li_2Mn_{2.9}Ni_{0.9}Co_{0.2}O_8$/MWCNT composite exhibits much higher discharge capacity than pristine $Li_2Mn_{2.9}Ni_{0.9}Co_{0.2}O_8$, which is quite interesting. Further, the discharge capacity of $Li_2Mn_{2.9}Ni_{0.9}Co_{0.2}O_8$/MWCNT cathode is found to be higher than the reported values of similar category cathodes [44, 45]. Based on this encouraging result, we have extended our study with a high current rate of 1C and found that the cathode delivers an exceptional discharge capacity of 240 mAh g^{-1} in the first cycle. Figure 5e shows the galvanostatic charge/discharge capacity –cycle number curve of $Li_2Mn_{2.9}Ni_{0.9}Co_{0.2}O_8$/MWCNT composite cathode at 1C current rate. At the end of the 100th cycle, the cathode delivers a capacity of 100 mAh g^{-1}, which is noteworthy. The coulombic efficiency of the title cathode is found to be 97% at 1C rate, which is the first of its kind observation. Figure 5f shows the rate capability behaviour of the title cathode at different current values ranging from C/10 to 5C. It is interesting to note that the cathode delivers an excellent capacity of 71 mAh g^{-1} even at 5C current rate. Appreciable tolerance against various rates such as 1C, 2C and 5C is evident from the figure. Further, the cell is switched back to the C/5 rate condition after

subjecting to a high current rate of 5C condition, it is capable of resuming the capacity value closer to 145 mAh g^{-1}, which is an indication of capacity retention behaviour. This in turn validates the suitability of $Li_2Mn_{2.9}Ni_{0.9}Co_{0.2}O_8$/MWCNT cathode for high rate applications, thus leaving ample scope to exploit wide variety of custom engineered spinel architectures for high rate lithium battery applications. Moreover, the capacity fading identified during 1C rate may be associated with the wide voltage range selected for the study and the structural reorganisation that occurs below 3V discharge. Capacity fading can be minimised by reducing the discharge cut-off voltage to 3.5 V and/or by increasing the amount of Ni^{2+} (which will be active above 4.5 V) and decreasing the concentration of Mn^{3+}.

Electrochemical impedance spectroscopy (EIS) measurements further confirm the advantageous effect of the interconnected MWCNTs in enhancing the electrochemical performance of the title cathode compared with that of bare $Li_2Mn_{2.9}Ni_{0.9}Co_{0.2}O_8$ cathode. The Nyquist plots of the pristine and composite cathode of $Li_2Mn_{2.9}Ni_{0.9}Co_{0.2}O_8$ are shown in Figure 6 wherein, an AC voltage of 10 mV amplitude in the frequency range of 0.25 MHz to 10 mHz has been applied. The high-frequency semicircle indicates favourable lithium transport kinetics. The diameter of the semicircle at the high

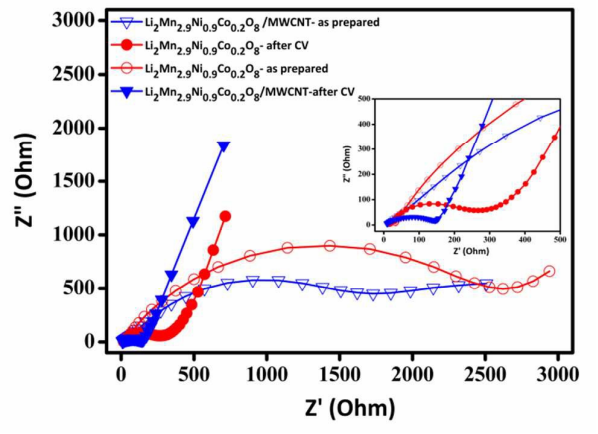

Figure. 6. Electrochemical Impedance Spectroscopy of pristine $Li_2Mn_{2.9}Ni_{0.9}Co_{0.2}O_8$ and $Li_2Mn_{2.9}Ni_{0.9}Co_{0.2}O_8$/MWCNT composite electrode, recorded before and after cycling.

frequency region of the as-fabricated pristine $Li_2Mn_{2.9}Ni_{0.9}Co_{0.2}O_8$ cathode and the corresponding $Li_2Mn_{2.9}Ni_{0.9}Co_{0.2}O_8$ /MWCNT composite electrode infers that the R_{ct} value of the composite (1700 Ω) is much lower than that of the pristine electrode (2700 Ω), which is in line with the conductivity values obtained with the pristine samples, prior to the electrochemical studies (SI, Figure S4). This is an indication of enhanced charge transfer, which is attributed to the conductive MWCNT network, decorating the surface of $Li_2Mn_{2.9}Ni_{0.9}Co_{0.2}O_8$ cathode material. The enhanced charge transfer kinetics of the composite cathode further confirms the increased contact area at the electrode/electrolyte interface and enhanced electrical conductivity resulting from the conductive MWCNT network. After five charge/discharge cycles, the cells have been subjected to EIS measurement and the Nyquist plots show decreased charge transfer resistance for both the electrodes, thus favouring high lithium diffusion kinetics. Hence, electrochemical impedance spectroscopy provides more insight on the stability of the chosen $Li_2Mn_{2.9}Ni_{0.9}Co_{0.2}O_8$/MWCNT cathode, especially upon lithiation and de-lithiation processes. Further, *ex situ* XRD studies were performed on $Li_2Mn_{2.9}Ni_{0.9}Co_{0.2}O_8$/MWCNT cathode with a view to confirm the structural stability of the same upon cycling. Interestingly, better correlation of structural integrity and electrochemical behavior has been obtained from *ex situ* XRD studies performed at different voltages. Four different cells have been fabricated and subjected to *ex situ* XRD with different cycling conditions. The as fabricated electrode shows the presence of all the possible diffraction peaks, corresponding to the spinel framework (Figure 7a). One cell has been stopped after initial de-lithiation or charge reaction and it is observed that the XRD pattern of the cathode material recovered from that cell shows a similar diffraction pattern as that of freshly fabricated $Li_2Mn_{2.9}Ni_{0.9}Co_{0.2}O_8$/MWCNT electrode, but with the decreased intensity of the (111) line, which is reduced especially upon charging (Figure 7b). Another cell was analysed after one complete cycle (one charge and one discharge), wherein the (111) line is found to resume the same intensity (Figure 7c).

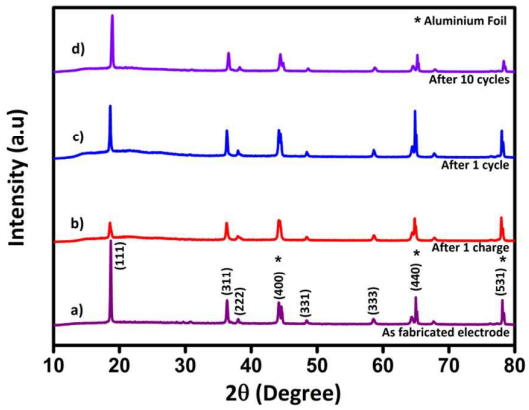

Figure. 7. *Ex situ* XRD pattern of $Li_2Mn_{2.9}Ni_{0.9}Co_{0.2}O_8$/MWCNT cathode recorded under different experimental conditions a) as fabricated electrode, b) electrode after one charge, c) electrode after one cycle and d) electrode after completing 10 cycles

This observation supports the complete reversibility of $Li_2Mn_{2.9}Ni_{0.9}Co_{0.2}O_8$/MWCNT cathode and facile diffusion of lithium ions upon lithiation and de-lithiation. More interestingly, the *ex situ* XRD pattern recorded for the cell after completing ten charge/discharge cycles shows striking similarity with that of the as fabricated electrode, thus substantiating the appreciable structural integrity and excellent cycling reversibility of $Li_2Mn_{2.9}Ni_{0.9}Co_{0.2}O_8$/MWCNT

cathode upon progressive cycling (Figure 7d). It is worth mentioning here that the XRD pattern derived lattice parameter value of *a*= 8.18 corresponding to the as-fabricated electrode has been found to show a minor deviation such as *a*= 8.176 upon de-lithiation or charge, driven by the slight change in the atomic radius upon oxidation process. However, after the completion of one cycle, the restored lattice parameter value of *a*= 8.18 has been observed, which is a strong evidence for the desired structural stability of $Li_2Mn_{2.9}Ni_{0.9}Co_{0.2}O_8$/MWCNT cathode.

4. Conclusion

In conclusion, we have synthesized a novel 5V category spinel cathode in the form of a composite, *viz*., $Li_2Mn_{2.9}Ni_{0.9}Co_{0.2}O_8$/MWCNT, wherein interweaving of individual nanoparticles of electro active material with multiwalled carbon nanotubes has been obtained by adopting a simple sonication approach. Herein, pristine $Li_2Mn_{2.9}Ni_{0.9}Co_{0.2}O_8$ spinel compound in the form of nanoflakes with *Fd3m* space group has been prepared by using template assisted co-precipitation method, followed by a solid-state reaction at 450 °C. Interestingly, $Li_2Mn_{2.9}Ni_{0.9}Co_{0.2}O_8$/MWCNT composite cathode exhibits good electrical conductivity, low charge transfer resistance and good structural stability upon cycling, as evidenced by the conductivity, electrochemical impedance spectroscopy and *ex situ* X-ray diffraction studies. The unique hetero structure of $Li_2Mn_{2.9}Ni_{0.9}Co_{0.2}O_8$/MWCNT composite cathode provides shorter lithium ion diffusion path and good electronic conductivity, resulting in the demonstration of excellent electrochemical properties. The title composite delivers a discharge capacity of ~210 mAh g^{-1} at 0.1C rate and an excellent rate capability at 1C rate with a specific discharge capacity of 100 mAh g^{-1}, facilitated by the exceptional structural stability. To our knowledge, this is the first ever report on the high capacity and high rate applicability of low temperature synthesized spinel category $Li_2Mn_{2.9}Ni_{0.9}Co_{0.2}O_8$/MWCNT composite, which in turn has been recommended as potential lithium intercalating cathode material through the present study. The promising results of this study open up a newer gateway to explore series of $Li_2MMn_3O_8$ spinel cathodes and the corresponding composites for exploitation in high capacity lithium batteries with rate capability.

Acknowledgements

P. Remith is grateful for the Inspire Fellowship support from Department of Science and Technology, India and N. Kalaiselvi acknowledges the support from MULTIFUN and TAPSUN projects funded by Council of Scientific and Industrial Research, India.

Notes and references

1 J. M. Tarascon and M. Armand, *Nature,* 2001, **414**, 359-367.
2 M. Armand and J. M. Tarascon, *Nature,* 2008, **451**, 652-657.
3 J. B. Goodenough and Y. Kim, *Chem. Mater.,* 2010, **22**, 587-603.
4 M. V. Reddy, G. V. Subba Rao, and B. V. R. Chowdari, *Chem. Rev*., 2013, **113**, 5364-5457.
5 C. Masquelier and L. Croguennec, *Chem. Rev*., 2013, **113**, 6552-6591.
6 A. M. Kannan, L. Rabenberg, A. Manthiram, *Electrochem. Solid-State Lett*., 2003, **6**, A16-A18.
7 I. D. Scott, Y. S. Jung, A. S. Cavanagh, Y. Yan, A. C. Dillon, S. M. George and Se-H. Lee, *Nano Lett.,* 2011, **11**, 414-418.
8 P. Barpanda, M. Ati, B.C. Melot, G. Rousse, J-N. Chotard, M-L. Doublet. M-T. Sougrati, S.A. Corr, J.C. Jumas and J-M. Tarascon, *Nat. Mater*., 2011, **10**, 772-779.
9 F. Wu, G. Tan, J. Lu, R. Chen, L. Li and K. Amine, *Nano Lett.,* 2014, **14**, 1281-1287.
10 H. Yu and H. Zhou, J. Phys. *Chem. Lett*., 2013**, 4**, 1268-1280.
11 N. Yabuuchi, K.Yoshii, S-T.Myung, I. Nakai and S. Komaba, *J. Am. Chem. Soc.,* 2011, **133**, 4404-4419.
12 Y. Lee, M. G. Kim and J. Cho, *Nano Lett.,* 2008**, 8,** 957-961.
13 M. M. Thackeray, S-H. Kang, C. S. Johnson, J. T. Vaughey, R. Benedek and S. A. Hackney, *J. Mater. Chem.,* 2007, **17,** 3112-3125.
14 Y. Sharma, N. Sharma, G.V. Subba Rao and B.V.R. Chowdari, *Solid State Ionics,* 2008, **179**, 587-597.
15 R. Wu , X. Qian , K. Zhou , J. Wei, J. Lou and P. M. Ajayan, *ACS Nano,* 2014, **8,** 6297-6306.
16 S. Ma, L. Sun, L. Cong, X. Gao, C. Yao, X, Guo, L. Tai, P. Mei, Y. Zeng, H. Xie and R. Wang, *J. Phys. Chem. C,* 2013, **117**, 25890-25897.
17 L. Shen, Q. Che, H. Li and X. Zhang, *Adv. Funct. Mater*., 2014, **24,** 2630-2637.
18 Q. Wang, X. Wang, B. Liu, G. Yu, X. Hou, D. Chen and G. Shen, *J. Mater. Chem. A,* 2013, **1**, 2468-2473.
19 T-F. Yi, Y-R. Zhu, X-D. Zhu, J. Shu, C-B. Yue and A-N. Zhou, *Ionics,* 2009, **15**, 779-784.
20 G. Q. Liu, L. Wen and Y. M. Liu, *J. Solid State Electrochem*., 10, **14,** 2191-2202.
21 W. Tang, Y. Hou, F. Wang, L. Liu, Y. Wu and K. Zhu, *Nano Lett*., 2013, **13**, 2036-2040.
22 K. R. Chemelewski , E-S. Lee, W. Li and A. Manthiram, *Chem. Mater*., 2013, **25**, 2890-2897.
23 X. Zhao, M. V. Reddy, H. Liu, S. Ramakrishna, G. V. Subba Rao and B. V. R. Chowdari, *RSC Adv.,* 2012, **2**, 7462-7469.
24 H. Kawai, M. Nagata, H. Kageyama, H. Tukamoto and A. R. West, *Electrochim. Acta,* 1999, **45**, 315-327.
25 H. Kawai, M. Nagata, H. Tukamoto and A. R. West, *J. Mater. Chem*., 1998, **8**, 837-839.
26 H. Kawai, M. Nagata, M. Tabuchi, H. Tukamoto and A. R. West, *Chem. Mater.,* 1998, **10**, 3266-3268.
27 R. I. Eglitis and G. Borstel, *Phys. Status Solidi A,* 2005, **202**, R13-R15.
28 C. J. Chen and M. Greenblatt, *J. Solid State Chem*., 1986, **64**, 240-248.
29 H. Kawai, M. Nagata, H. Tukamoto and A. R. West, *Electrochem. Solid-State Lett*., 1998, **1**, 212-214.
30 H. Kawai, M. Nagata, H. Tukamoto and A. R. West, *J. Power Sources,* 1999, **81–82**, 67-72.
31 H. K. Noh, H-S. Park, H. Y. Jeong, S. U. Lee and H-K. Song, *Angew. Chem. Int. Ed.,* 2014, **53,** 5059-5063.
32 S. Lee, Y. Cho, H-K. Song, K. T. Lee and J. Cho, *Angew. Chem. Int. Ed*., 2012, **51,** 8748-8752.
33 V. N. Kislenko and L. P. Oliynyk, *J. Polym. Sci., Part A: Polym. Chem.,* 2002, **40**, 914-922.
34 Y. M. Sultanov, D. Wohrle and A.A. Efendiev. *J. Mol. Catal. A: Chem.,* 2006, **258**, 77-82.
35 J. Dai and M. L. Bruening, *Nano Lett.,* 2002, **2**, 497-501.
36 X. Zhang, F. Cheng, K. Zhang, Y. Liang, S. Yang, J. Liang and J. Chen, *RSC Adv*., 2012, **2**, 5669-5675.

37 L. Zhou, D. Zhao and X. W. (David) Lou, *Angew. Chem. Int. Ed.,* 2012, **51,** 239-241.
38 Y. Xue, Z. Wang, F. Yu, F. Zhang and G. Yin, *J. Mater. Chem. A*, 2014***, 2,*** 4185-4191.
39 L. Wang, H. Li, X. Huang and E. Baudrin, *Solid State Ionics,* 2011, **193**, 32-38.
40 Y. Talyosef, B. Markovsky, G. Salitra, D. Aurbach, H.-J. Kim and S. Choi, *J. Power Sources,* 2005*,* **146***,* 664-669.
41 J. Xiao, X. Chen, P.V. Sushko, M. L. Sushko, L. Kovarik, J. Feng, Z. Deng, J. Zheng, G. L. Graff, Z. Nie, D. Choi, J. Liu, J-G. Zhang and M. S. Whittingham, *Adv. Mater.,* 2012, **24,** 2109-2116.
42 J. C. Arrebola, A. Caballero, M. Cruz, L. Hernán, J. Morales and E. R. Castellón, *Adv. Funct. Mater.,* 2006, **16,** 1904-1912.
43 A. Manthiram, K. Chemelewski and E-S. Lee, *Energy Environ. Sci*., 2014, **7**, 1339-1350.
44 X. Jia, C. Yan, Z. Chen, R. Wang, Q. Zhang, L. Guo, F. Wei and Y. Lu, *Chem. Commun*., 2011, **47**, 9669-9671.
45 D. K. Kim, P. Muralidharan, H-W. Lee, R. Ruffo, Y. Yang, C. K. Chan, H. Peng, R. A. Huggins and Y. Cui, *Nano Lett*., 2008, **8**, 3948-3952.

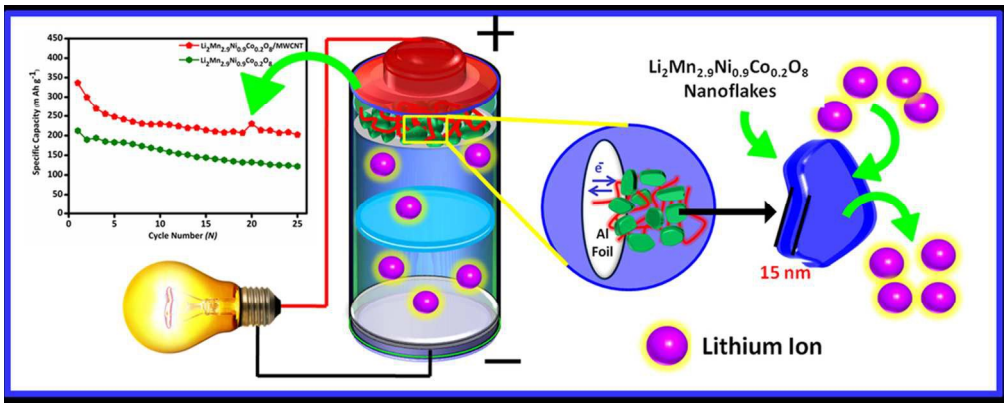

97x38mm (300 x 300 DPI)